American Journal of Remote Sensing
2021; 9(1): 1-15
http://www.sciencepublishinggroup.com/j/ajrs
doi: 10.11648/j.ajrs.20210901.11
ISSN: 2328-5788 (Print); ISSN: 2328-580X (Online)

Methodology Article

Balancing Land Surface's Brightness-Shadowing and Spectral Reflectance to Enhance the Discrimination of Built-up Footprint from Surrounding Noise

Alfred Homere Ngandam Mfondoum[1, 2, *], Paul Gerard Gbetkom[3], Sofia Hakdaoui[4], Ryan Cooper[5], Armel Fabrice Mvogo Moto[2, 6], Brian Njumeneh[6]

[1]StatsN'Maps, Private Consulting Firm, Dallas, USA

[2]Laboratory of Natural Resources Management, Department of Geography, University of Yaounde I, Yaounde, Cameroon

[3]Department of Geography, University of Aix-Marseille, Marseille, France

[4]Geoscience, Water and Environment Laboratory, Faculty of Sciences, Mohammed V University in Rabat, Av. Ibn Batouta, Rabat, Morocco

[5]Erik Jonsson School of Engineering and Computer Science, University of Texas in Dallas, Richardson, Texas, USA

[6]I Love Geomatics Association, Yaoundé, Cameroon

Email address:

stats.n.maps.expertise@gmail.com (A. H. N. Mfondoum), Alfred.homere@gmail.com (A. H. N. Mfondoum), ggbetkom@gmail.com (P. G. Gbetkom), s.hakdaoui@um5r.ac.ma (S. Hakdaoui), Rdc190001@utdallas.edu (R. Cooper), ilovegeomatics@yahoo.fr. (A. F. M. Moto)

[*]Corresponding author

To cite this article:

Alfred Homere Ngandam Mfondoum, Paul Gerard Gbetkom, Sofia Hakdaoui, Ryan Cooper, Armel Fabrice Mvogo Moto, Brian Njumeneh. Balancing Land Surface's Brightness-Shadowing and Spectral Reflectance to Enhance the Discrimination of Built-up Footprint from Surrounding Noise. *American Journal of Remote Sensing*. Vol. 9, No. 1, 2021, pp. 1-15. doi: 10.11648/j.ajrs.20210901.11

Received: December 14, 2020; **Accepted**: December 25, 2020; **Published**: January 4, 2021

Abstract: Recent evolutions of the geospatial technologies are more accurate in mapping and monitoring land use land cover, LULC, in different environments and at different spatial scales. However, some urban applications keep facing issues such as misclassification and other noise in unplanned cities with disorganized built-up and mixed housing material, and surrounded by a composed biophysical environment. This paper reports the processing leading to a new spectral index, that balances the land surface brightness temperature and spectral reflectance to accurately extract the built-up. The namely Brightness Adjusted Built-up Index, BABI, is proposed as a weighted ratio of Landsat OLI-TIRS bands. The methodology is based on a multi-perceptron layers, MLP, regression between a classified image and individually classified red, SWIR1, SWIR2 and TIR bands reclassified "1 = built-up; 0 = Non-Built-up", with an average r^2=0.78. The same way, a linear regression of popular built-up spectral indices such as Normalized Difference Built-up Index, NDBI, and Urban Index, UI, or recently proposed Modified New Built-up Index, MNBI, and Normalized Difference Built-up and Surroundings Unmixing Index, NDBSUI, on one hand, by light-dark spectral indices such as, Normalized Difference Soil Index, NDSI, Bare Soil Index, BSI, and Shadow index on the other hand, stands for the natural environment noise assessment in and around the built-up, with an r^2=0.75. The MLP r^2 standing for the built-up information, is rounded to 0.8 and according to their rank in the process, the weights allotted are 0.2, 0.4 and 0.8 in the numerator, and inversely 0.8, 0.6 and 0.2 in the denominator, to the red, SWIR1 and SWIR2 bands respectively. Whereas, the simple linear regression r^2 standing for the noise is used to weigh the brightness temperature, T_B in the numerator and subtracted from the previous group. The value 0.001 multiplies the whole ratio to lower the decimals of the outputs for an easy interpretation. As results, on the floating images scaled [0-1], built-up values are ≥0.1 in Yaoundé (Cameroon) and ≥0.07 in Bangui (Central African Republic). The overall accuracies are 96% in Yaoundé and 98.5% in Bangui, with corresponding kappa coefficients of 0.94 and 0.97. These scores are better than those of the NDBI, UI, MNBI and NDBSUI.

Keywords: Brightness-shadowing, Built-up, Multi-Layers Perceptron, Linear Regression, Noise, Unplanned Cities

1. Introduction

1.1. Background, Problem Statement and Study Area

Nowadays, the satellite imagery is a powerful and reliable tool to assess the global urban footprint [1]. One set of useful techniques include the image classification according to different algorithms [2-5]. These methods consider the shape, the size, the context as well as the spectral content, and are consequently important when the satellite image used has a very high resolution (VHR) [5]. Besides, the use of spectral indices has also been successful in mapping the built-up and urban impervious area with high accuracies. Pillar ones are the urban index, UI, [6] and the normalized difference built-up index, NDBI [7], that respectively enable the residential areas and the human settlements automatic mapping using simple ratios between two spectral channels. They were followed by several other spectral indices giving similar or higher accuracies depending on the test area [8-19].

However, these applications are enough challenging in the rapid and unplanned urbanization context of many developing countries. Amongst several reasons, one can mention the extent of slums built with recovery materials (plastics, sheet metal, etc.) inside cities and along asphalted or dusty roads, as well as suburbanization that blurs the limits of modern built-up and craft made housing. It has been noticed that the pixel combinations in areas with heterogenic objects [13, 22, 23] causes high rate of uncertainties and biases [9, 23-25]. Moreover, spectral signatures of impervious surface areas are similar to those of dry soils [10, 11], whereas detecting surface water is a challenge in regard of its confusion with buildings' shadowing [24].

For illustration, some of these applications were tested in sub-Saharan Africa, specifically the urbanized areas of Yaoundé (Cameroon) and Bangui (Central African Republic) (Figure 1). These cities have a common urban mixed structure, i.e., planned and unplanned build area. Their natural surroundings also have some similarities such as internal forest, gardens, savannahs or shrubs for vegetation, lakes, streams, or swamps for water bodies, rocky, dusty or sandy bare soils, and rough or mountainous terrain, which are spectrally noisy for the built-up extraction (Figure 2). On the Landsat 8 subsets extracted for the study, vegetation and built-up are dominant in Yaoundé, while bare soils, rough terrain and water bodies are added to the two previous land cover classes in Bangui (Figures 1&3).

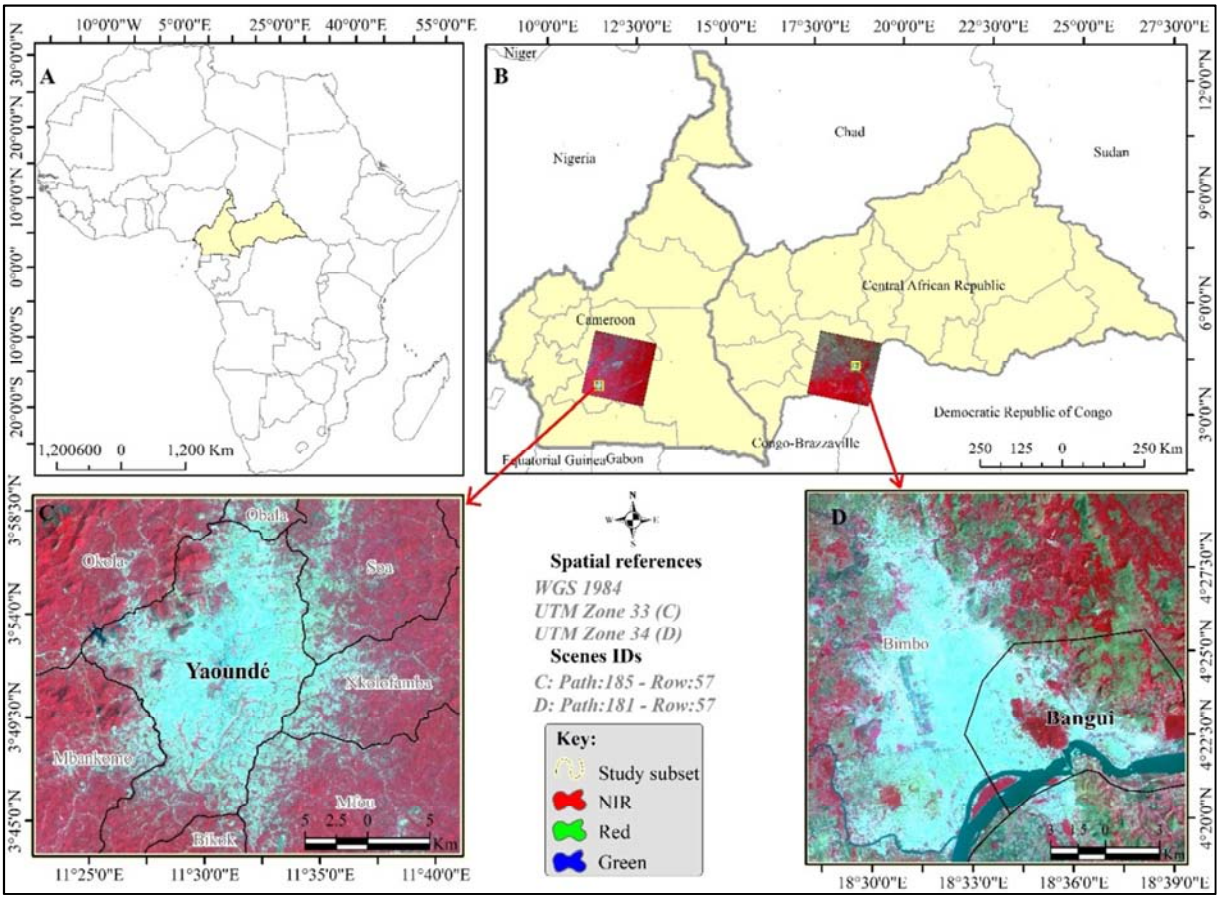

Figure 1. *The study location. Cameroon and Central African Republic (A&B); subset of Yaoundé and surroundings (C); subset of Bangui and surroundings (D).*

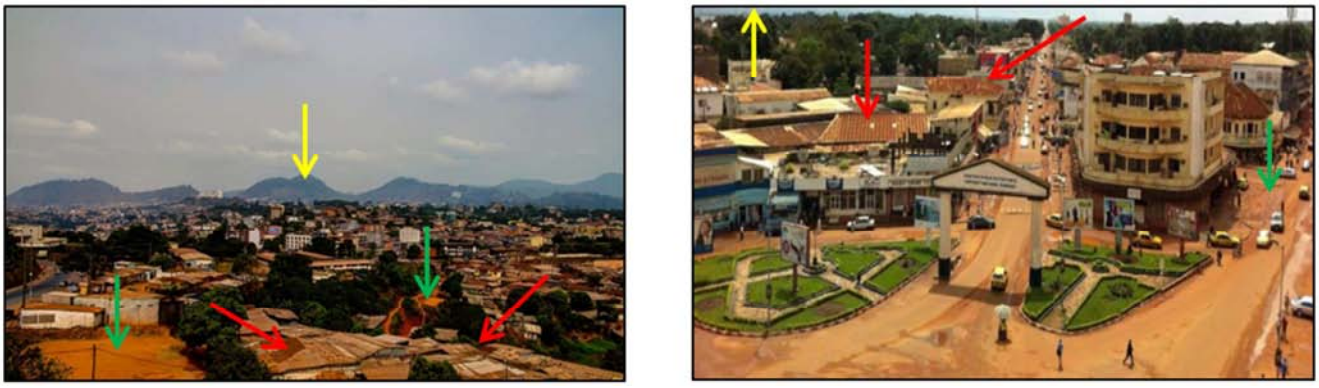

Figure 2. *Partial cityscape view of Yaoundé (A) and Bangui (B). The mixing of modern new and old buildings, the nearness of rusty rooftops (red arrow) and unpaved dusty/muddy roads/spaces (green arrow), and the rough terrain (yellow arrow) are some sources of satellite image misclassification. [Source: Yaoundé (dreamstime.com) and Bangui (sangonet.com)].*

On one hand, the combination of these conditions at different levels usually impact the discrimination of built-up from the other land cover features as noticed on the patterns of the NDBI [7] and the Normalized Difference Impervious Surface Index, NDISI [10] (Figure 3). Thus, although their original goals are the urban built-up mapping, the NDISI inverts the visual patterns of NDBI by highlighting dark impervious surfaces and water bodies.

On the other hand, the high values of land surface temperature, LST, are a mix of built-up and bare soils trends in the two sites. For the case of Bangui, several built-up hot spots even record medium to low LST values (Figure 3).

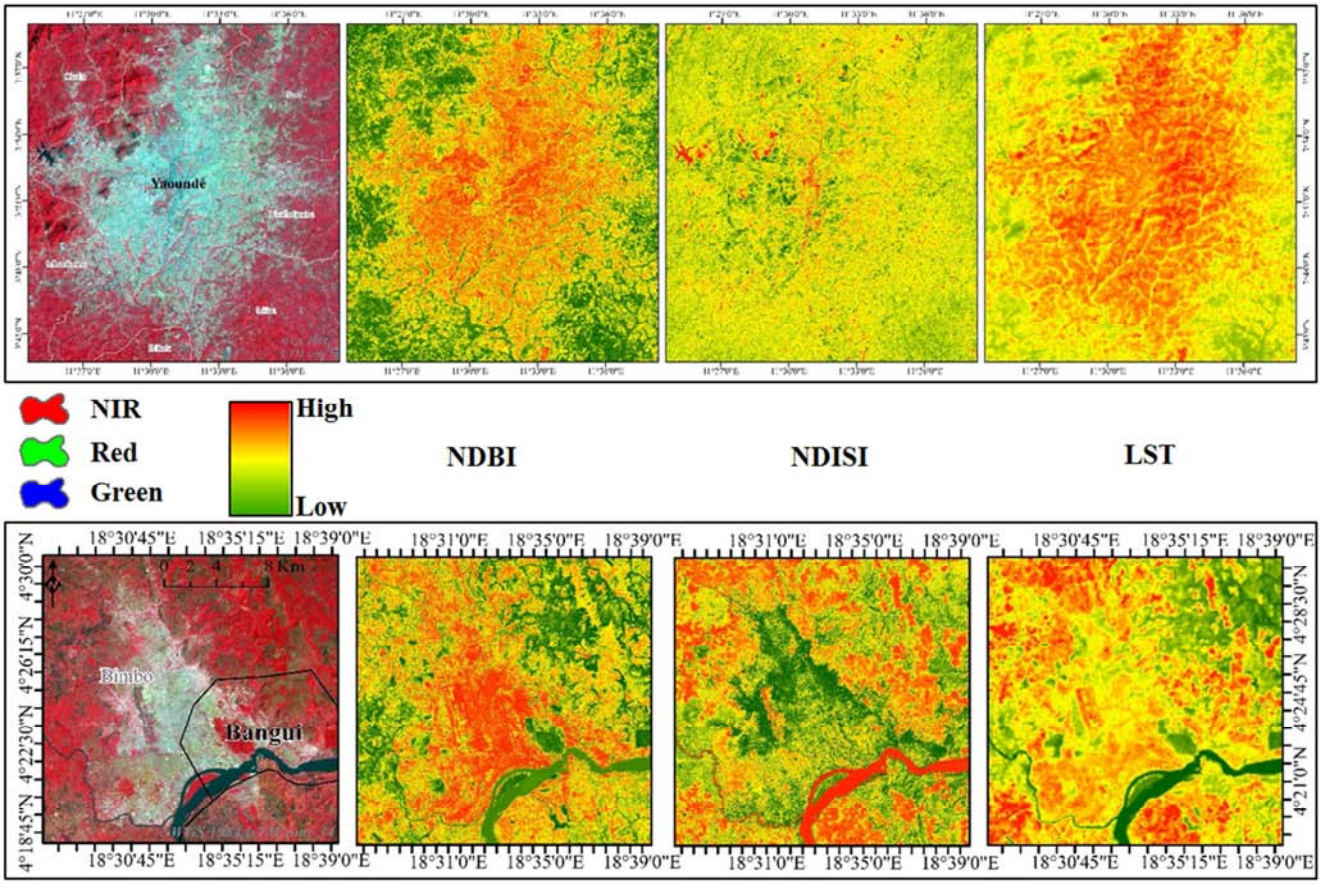

Figure 3. *Some popular built-up and urban spectral indices and methods tested in Yaoundé and Bangui.*

Fundamentally, the land surface temperature, LST, enables the mapping of urban heat islands (UHIs) [20, 21]. However, it is highly influenced in its interactions with the climate, by the land features distribution [25-29]. Figure 4 supports this statement by showing a high positive correlation of LST with both built-up and soil features, detected through spectral indices (Table 1).

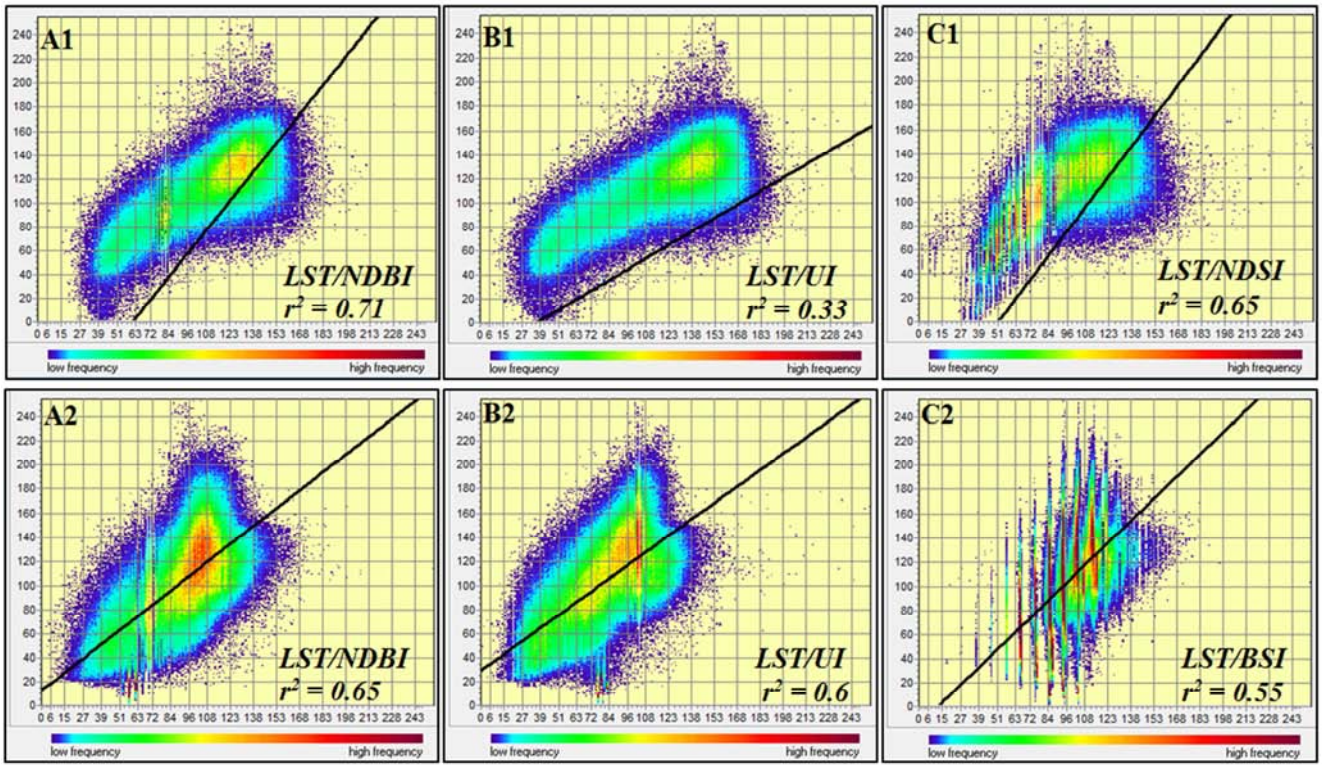

Figure 4. *Relation of LST with built-up and bare soil – Yaoundé (A1-C1) and Bangui (A2-C2). Bare soil index, BSI [30], and normalized difference soil index, NDSI [31].*

Table 1. *The indices used for mapping and linear regression.*

Index	Feature targeted	Expression based on Landsat OLI-TIRS sensors	Reference
UI	Urban Settlements	$\frac{SWIR2 - NIR}{SWIR2 + NIR}$	[6]
NDBI	Built-up	$\frac{SWIR1 - NIR}{SWIR1 + NIR}$	[7]
NDISI	Impervious surfaces	$\frac{\left[T_b - \frac{MNDWI+NIR+SWIR1}{3}\right]}{\left[T_b + \frac{MNDWI+NIR+SWIR1}{3}\right]}$, with $MNDWI = \frac{Green-SWIR1}{Green+SWIR1}$	[10]
BSI	Forest areas bare soils	$\frac{(SWIR2 + Red) - (NIR + Blue)}{(SWIR2 + Red) - (NIR + Blue)}$	[30]
NDSI	Urban and Suburban soils	$\frac{SWIR1 - Green}{SWIR1 + Green}$	[31]

1.2. Previous Experimentations

To address these issues, we recently experimented two new indices based on spectral bands arithmetic and they have been successfully applied in six different cities of Cameroon. The first one is the modified New Built-up Index, MNBI, to enhance the built-up extraction and analyse the spatiotemporal urban metabolism of Foumban (West-Cameroon) [32]. It uses the Landsat 8 images and enhances the NBI [8] results, by using the following algorithm:

$$MNBI = \sqrt{NBI^2 + \rho SWIR2^2} \text{ [32]}$$

Where, $NBI = \frac{\rho Red * \rho SWIR1}{\rho NIR}$ [8] and ρ is the land surface reflectance of Landsat OLI-TIRS designated band. On the image of 2019 in Foumban, the MNBI was efficient in the built-up extraction with an overall accuracy (OA) of 95.3% and a kappa coefficient (KC) of 0.93.

The recent proposal is the Normalized Difference Built-up and Surroundings Unmixing Index, NDBSUI, to automate the built-up extraction in five different biophysical environments [33]. Its detailed goal has been to extract the built-up features and interweave its spectral signal from surrounding noise. Therefore, still using the Landsat 8 image to, the algorithm was proposed as follows:

$$NDBSUI = \frac{\left(\rho SWIR2 + \sqrt{\rho Red * \rho SWIR1}\right) - (\rho Red + \rho SWIR1)}{\left(\rho SWIR2 + \sqrt{\rho Red * \rho SWIR1}\right) + (\rho Red + \rho SWIR1)} \text{ [33]}$$

On Landsat 8 satellite images of 2019, the outcomes view was better and the overall accuracies higher than comparative indices, i.e., OA=95.5% (KC=0.90) in the main study area of Yaoundé (humid forest). In the validation sites, they were the following: Yokadouma (humid forest) OA=98.9% (KC=0.88); Kumba (humid Mountainous forest) OA=97.5% (KC=0.94); Foumban (highlands savannah) OA=97.06% (KC=0.92); Ngaoundéré (high guinea savannah) OA=95.3% (KC=0.89); Garoua (sudano-sahelian shrubs) OA=74.86% (KC=0.42).

As a continuum, this research focuses on reducing the noise created by the land surface brightness and shadowing, while mapping built-up. The goal is to improve the accuracy of built-up extraction, while inhibiting the reflectance of natural features (vegetation, bare soil, water body) as well as buildings shadows, dark paved (asphalts) or unpaved (dusty/muddy) roads.

2. Materials and Methods

2.1. Satellite Images Acquisition

The satellite images of Landsat operational land imager and thermal infrared sensor, OLI-TIRS, were downloaded for the dry season (Table 2), from the website of United States Geological Survey (USGS). This phenological season is responsible of the highest level of soil bareness and rough terrain brightness/shadowiness around and in between the buildings, highlighting the issue of the land cover object confusions to be solved. Some visible and thermal infrared bands were used (Table 3).

Table 2. *Identification of the images used.*

Site	Scene ID	Month
Yaoundé	LC81850572020026LGN00	February
Bangui	LC81810572020014LGN00	January

Both scenes were first pre-processed for atmospheric correction, conversion to radiance, and then to at-sensor reflectance for OLI bands using the LOW-COST model [37], and to brightness temperature for the thermal infrared band 10 following the steps proposed by references [38, 39].

Table 3. *Landsat OLI-TIRS characteristics.*

Resolution (m)	Band name	Wavelength (μm)
30	Coastal/Aerosol	0.435 – 0.451
	Blue	0.452 – 0.512
	Green	0.533 – 0.59
	Red	0.636 – 0.673
	NIR	0.851 – 0.879
	SWIR1	1.566 – 1.651
	SWIR2	2.107 – 2.294
15	Panchromatic	0.503 – 0.676
30	Cirrus	1.363 – 1.384
100	TIR-1	10.60 – 11.19
	TIR-2	11.50 – 12.51

2.2. Spectral Measures

Based on 100 to 200 pixels sampled 40 at least at a time, spectral signatures of built-up, vegetation, bare soil and water body have been plotted and assessed. As shown in figure 5, SWIR1 and SWIR2 bands give the highest reflectance for built-up that stands in this study for the bright impervious surfaces. However, vegetation, soil and water reflectance are closer to the built-up in the SWIR1 (Vegetation=[16-18]%; Soil =[17-18]% Water=[11-15]%; Built-up=[20-21]%), than they are in the SWIR2 (Vegetation=[10-12]%; Soil=[14-15]%; Water=[9-12]%; Built-up=[17-18]%) (Figure 5). The difference of reflectance between the built-up and other features is 6%, 3% and 6% for vegetation, soil and water in the SWIR2, versus 3%, 3% and 6% in the SWIR1 for the same order of appearance. The same way, the TIR band shows an increasing (in Yaoundé) or decreasing (in Bangui) trend of these features, emphasizing the questioning about its ability for built-up detection.

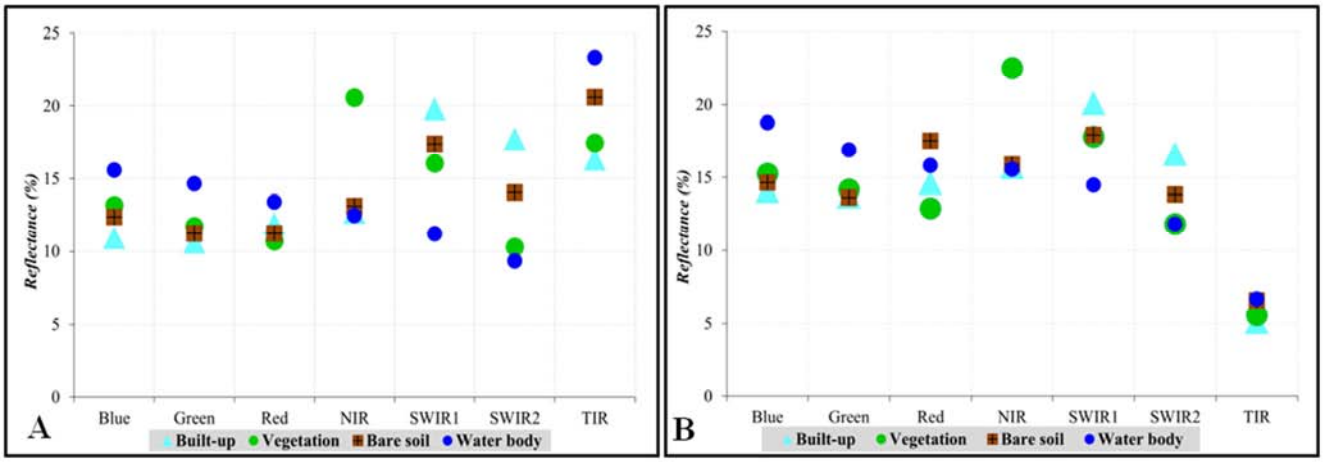

Figure 5. *Spectral reflectance of LULC in Yaoundé (A) and Bangui (B).*

As a reminder, reference [40] experienced that Landsat 8 images in-band and out-of-band measured spectral response for vegetation and soil, shows a lack of spectral uniformity between the radiance of the red, SWIR1 and SWIR2 bands. Indeed, the maximum and average radiance of soil is uniform, constant and continued in the red and SWIR1 bands, while it records the highest discontinuity in the SWIR2, then explaining the difference of reflectance previously mentioned.

In addition, recent studies noticed that the thermal infrared data is able to support the processing separating water bodies from impervious surfaces, yielding an identifiable temperature difference between them [41]. Whereas it was pointed out that bare soil has spectral response patterns highly similar to high-albedo (HA) impervious surfaces that is obtain by using TIR band [42, 43].

2.3. Built-up Information in Spectral Bands and the First Experimental Assumption

Two complementary regressions are performed to predict the informational rate of built-up features. The first one uses the Multi-Layer Perceptron, MLP. It is a class of feed forward artificial neural network, ANN, that is known as a connected network of processing units that are modelled on the most basic properties of the neurons in the human brain and has been satisfactorily used in several fields of research including remote sensing [44, 45]. MLP utilizes a supervised learning technique called backpropagation for training [46]. Its multiple layers and non-linear activation distinguish MLP from a linear perceptron. In addition, it performs a non-parametric regression analysis between input variables and one dependent variable with the output containing one output neuron, i.e., the predicted memberships. For this later method, the values of the output predicted image is the activation level of the output layer node scaled to the original data range, which is expressed as follows:

$$o_k = f(net_k), \text{ with, } net_k = \sum_{j-1}^{n} w_{jk} o_j$$

Where f symbolizes the activation function, w and o are the weights and the biases.

Using the K-means processing, an unsupervised classification was performed for the stacked image and for the individual bands red, SWIR1, SWIR2 and TIR. The results were converted in 2bits (binary), with *1* for the built-up and *0* for the other classes. Then, a MLP network (Figure 6) logistic sigmoidal regression was implemented, inputting the classified individual bands as independent variables and the classified stacked image as dependent variable. Using an automatic training process, a total of 1000 pixels were defined for the learning, i.e., 500 for training and 500 for the testing, for a processing cycle of 1000 iterations (Figure 7). In Yaoundé, the r^2 of the model is *0.84* versus *0.73* for Bangui (Table 4). When assessing the sensitivity of the model, the constancy of the r^2 identifies the red band as *'least influential'* with *0.84*, and the SWIR2 as *'most influential'* with *0.48* in Yaoundé, and in the same order, the values recorded in Bangui are *0.72* and *0.012* (Figure 7&Table 5).

The second set of regressions are the simple linear ones. Their trends confirm the presence of built-up features in each classified band, with the highest r^2 for the SWIR2, i.e., 0.84 in Yaoundé and 0.8 in Bangui, and the lowest ones for the TIR, i.e., respectively 0.75 and 0.47 in the same order. (Figure 8).

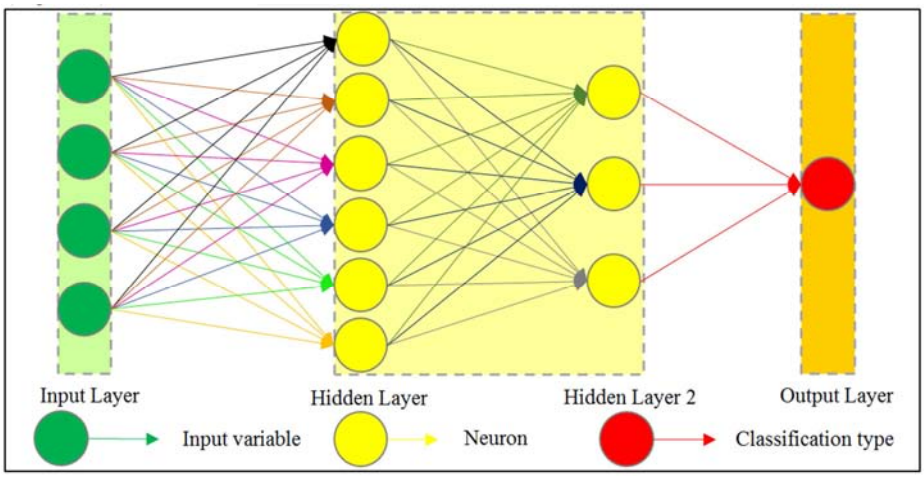

Figure 6. *Architecture of the MLP regression used.*

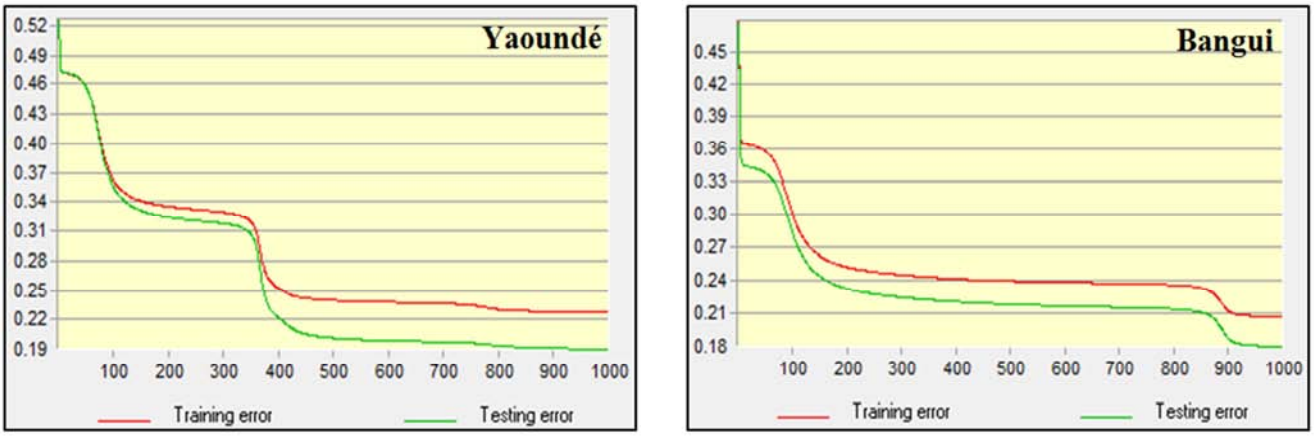

Figure 7. *Sensitivity analysis of the model, based on 1000 iterations duration.*

Table 4. *Parameters and performance of the MLP regression.*

Yaoundé		**Bangui**	
Application type	***Regression***	***Application type***	***Regression***
Input layer neurons	4	Input layer neurons	4
Hidden layers	2	Hidden layers	2
Hidden layer 1 neurons	6	Hidden layer 1 neurons	6
Hidden layer 2 neurons	3	Hidden layer 2 neurons	3
Output layer neurons	1	Output layer neurons	1
Maximum requested samples	1000	Maximum requested samples	1000
Final learning rate	0.0100	Final learning rate	0.0100
Momentum factor	0.5	Momentum factor	0.5
Sigmoid constant	1	Sigmoid constant	1
Acceptable RMS	0.01	Acceptable RMS	0.01
Iterations	1000	Iterations	1000
Training RMS	0.2278	Training RMS	0.2068
Testing RMS	0.1907	Testing RMS	0.1799
R square	0.8372	R square	0.7267

Table 5. *Sensitivity of the model to forcing a single independent variable to be constant (i) and all independent variables except one to be constant (ii).*

Model	**Yaoundé**			**Bangui**		
	r^2 ***(i)***	r^2 ***(ii)***	***Order***	r^2 ***(i)***	r^2 ***(ii)***	***Order***
With all variables	0.8372	0.8372	N/A	0.7267	0.7267	N/A
Var. 1 constant (Red)	0.8376	0.0000	4	0.7251	0.0881	4
Var. 2 constant (SWIR1)	0.5404	0.0000	2	0.7262	0.0000	2
Var. 3 constant (SWIR2)	0.4871	0.0743	1	0.0117	0.7247	1
Var. 4 constant (TIR)	0.7199	0.0000	3	0.7269	0.0000	3

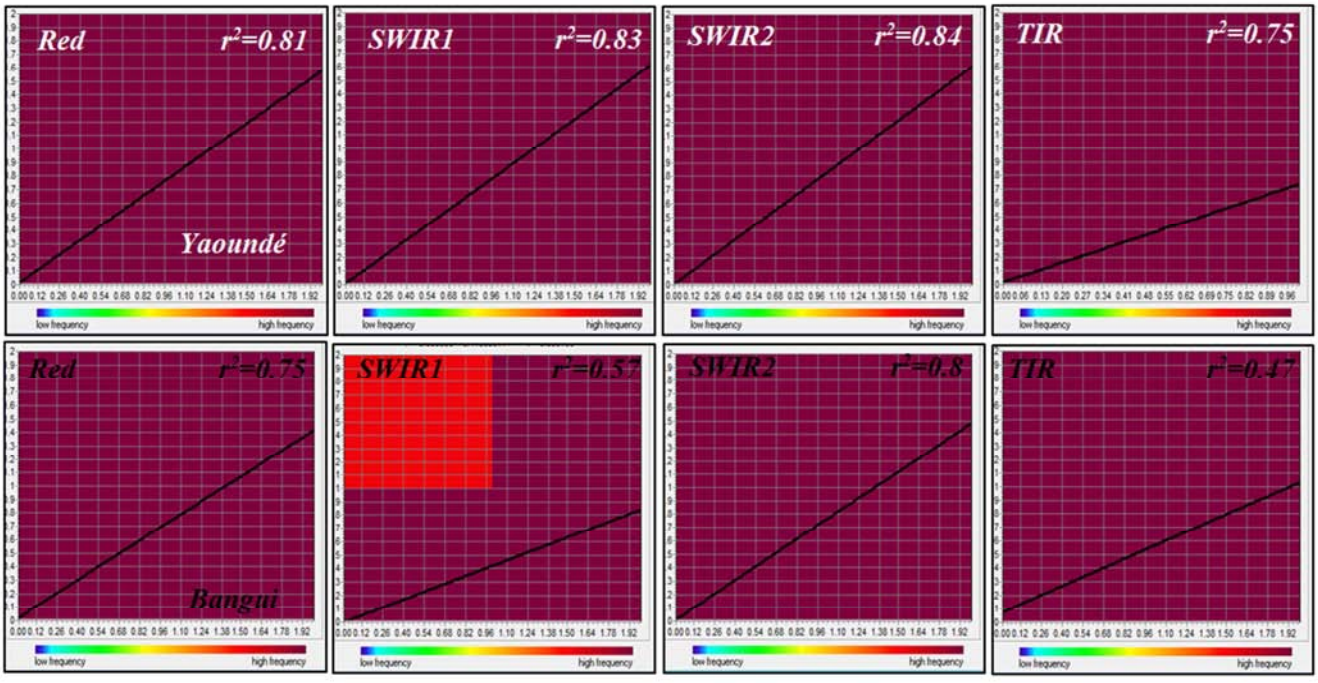

Figure 8. *Relation between the built-up classes detected on classified stacked images and individual bands.*

From the observations above, the first assumption is stated as follows: i) *ratio of the predicted built-up information over the predicted noise might be able to extract at best the built-up features*. The r^2 values resulting from the MLP model regression and the ordering of the variables resulting from the analysis of the sensitivity model are favourable to the respective decreasing weighing SWIR2, SWIR1, TIR and Red to influence the built-up extraction.

Then remains to determine the type and predict the level of noise, as well as its influence in the discrimination of built-up features. This infers their spectral and statistical relations.

2.4. Noise Prediction and the Second Experimental Assumption

Noise can be categorized as brighter and darker bodies, in and around the built-up. To assess its influence, the most accurate bare soil index, BSI [30] for Bangui and NDSI [31] for Yaoundé, and the shadow index [36] are each regressed by four urban/built-up, spectral indices, i.e., UI [6], NDBI [7],

MNBI [32] and NDBSUI [33]. These regressions are positive with the BSI/NDSI and negative with the shadow index. The average correlation coefficient r^2 are *0.74* for both bright and dark noise on the two study sites (Table 6). It can be noticed that in Yaoundé, the bright noise (NDSI) is more effective with r^2 of *0.8* versus -*0.68* for the dark noise (SI). While in Bangui, these r^2 record a slight difference, with respectively *0.75* (BSI) and -*0.73* (SI).

For further confirmation, the BSI [30], NDSI [31] and the shadow index [36] are also regressed by the brightness temperature, T_B, extracted from the thermal infrared band 10 (Read about detailed processing in references [20, 21]). The correlation coefficients r^2 are *0.51* (NDSI) and -*0.32* (SI) in Yaoundé, for -*0.95* (BSI) and *0.23* (SI) in Bangui (Table 6).

The second assumption at this point is the following: ii) *the average r^2 values resulting from the linear regression between NDSI/BSI and SI can be used to weigh T_B, and then subtracted from the sum of weighted red, SWIR1 and SWIR2 bands*. This should result in isolating surrounding noise, whilst enhancing the built-up detection and discrimination.

Table 6. *R square values predicting the rate of noise.*

	Yaoundé			**Bangui**		
	Bright noise (NDSI)	***Dark noise (SI)***	***|Average|***	***Bright noise (BSI)***	***Dark noise (SI)***	***|Average|***
NDBI	0.96	- 0.85	0.9	0.77	- 0.84	0.8
UI	0.88	- 0.82	0.85	0.81	- 0.74	0.77
MNBI	0.88	- 0.64	0.76	0.72	- 0.75	0.73
NDBSUI	0.48	- 0.41	0.44	0.71	- 0.6	0.65
|Average|	0.8	0.68	0.74	0.75	0.73	0.74
T_B	0.51	- 0.32		- 0.95	0.23	

2.5. Summative Processing-the Brightness Adjusted Built-up Index, BABI

The outflow of preparatory processing above is an algorithm expressed as a ratio. The weights are affected differently at the numerator and the denominator. The average r^2 of the two sites resulting from the MLP model, i.e., *0.78* rounded to *0.8*, is used to deduct a weight (*w*) for each visible band, exempting the TIR that is assumed still noisy. Therefore, to fill the gap in ranks and values caused by the previous assumption, for the numerator, the average r^2 is divided by 4 for red band (' *least influential variable*'; *w=0.18≈0.2*), by 2 for the SWIR1 (*w=0.39≈0.4*), and by *1* for the SWIR2 (' *most influential variable*'; *w=0.78≈0.8*). These weights are the estimated quantity of built-up information in the considered band.

The inverse and compensatory weights are used in the denominator, such as *0.8*, *0.6* and *0.2* for red, SWIR1 and SWIR2 bands respectively. These weighs stand for the quantity of noise in each band.

Concerning the T_B, its weights were given such as *0.74≈0.75* in the numerator and *1* in the denominator. The first weight is the predicted noise and the second weight stands for the entire information in the T_B.

In this form, the difference of weights between numerator and denominator as well as the usual high values of the T_B will induce high number of decimals that will be at the nearest thousandth. Therefore, an ε value, *0.001*, is introduced as a factor of the whole above operations to ease the results' interpretation.

From the above process, the Brightness Adjusted Built-up Index, BABI, is generated as a weighted ratio in the following formula:

$$BABI = \left[\left(\frac{[(0.2 * \rho Red) + (0.4 * \rho SWIR1) + (0.8 * \rho SWIR2)] - [0.75 * T_B]}{[(0.8 * \rho Red) + (0.6 * \rho SWIR1) + (0.2 * \rho SWIR2)] + T_B} \right) * 0.001 \right]$$

3. Results

3.1. Built-up Extraction Efficiency

Figure 9 shows the maps of built-up extraction by the proposed method and following the first goal of this study. The BABI is stretched [*0.047–1.452*] in Yaoundé, with the main information concentrated between [*0.05–0.4*], versus [*0.014–0.76*] and [0.015–0.18] for the same purposes in Bangui. The built-up extraction is more efficient when compared to the classification map (Figure 9).

For a background analysis, the *Jenks* natural breaks were used as automatic classifier. This method helps to reduce variance within groups and maximize variance between groups. Four natural breaks were applied on the raw floating results (Figure 10), and the thresholds for built-up features are ≥ 0.18 for Yaoundé and ≥ 0.074 for Bangui. Similar steps were used after the images were rescaled [0-1], thresholding the built-up extraction at ≥ 0.1 in Yaoundé and ≥ 0.075 in Bangui (Figures 9 &10). This distribution of values reduces the built-up features generalization with satisfactory visual appraisal when compared with classification and other spectral indices (Figure 9).

One important point is about the compensatory effects between sub-information and over-information. For instance, when using the class separability matrix detailed in table 7, the classification in both sites presents confusion between bare soils and built-up classes. Thus, the values of the separability between the built-up and the bare soils are not only the lowest, i.e., *47.9* in Yaoundé and *41.8* in Bangui, but they are also way below the best average separability, respectively sets at *60.8* and *57.9*. Visually, while the classification of Yaoundé is over-informative in and around the built-up, the one of Bangui presents a low built-up detection compared to the RGB image and the BABI. Overall, on the two sites, the NDBSUI, MNBI, NDBI and UI are over-informative compared to the BABI

(Figure 9).

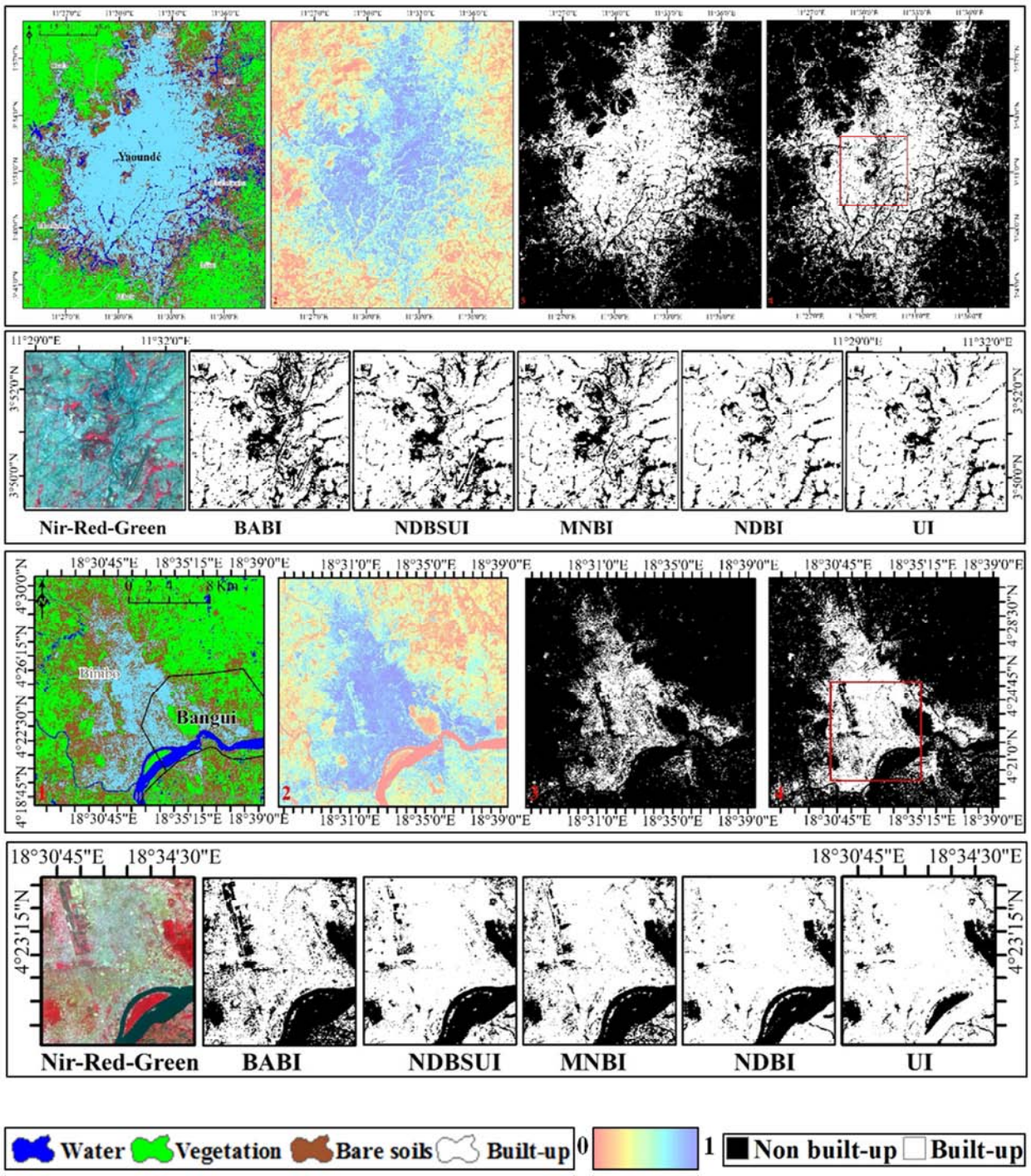

Figure 9. *Comparative patterns of BABI. The raw classification (1) and the BABI stretched [0-1] (2) show the same trends for built-up. Their binary versions, i.e., classification (3) and thresholds of BABI (4) show the built-up footprints. On urban zooms (red square, rows 2 and 4), the BABI is efficient than compared spectral indices in reducing both high and low reflectance noise.*

Table 7. *Spectral signatures/classes separability.*

Signatures	Yaoundé				Bangui			
	Built-up	***Vegetation***	***Bare soil***	***Water Body***	***Built-up***	***Vegetation***	***Bare soil***	***Water Body***
Built-up	0	71.7031	47.9331	101.971	0	57.7493	41.8391	97.7805
Vegetation	71.7031	0	32.5667	54.4132	57.7493	0	32.4568	60.6467
Bare soil	47.9331	32.5667	0	56.6885	41.8391	32.4568	0	57.0011
Water Body	101.971	54.4132	56.6885	0	97.7805		57.0011	0
Best Average Separability: 60.8792					Best Average Separability: 57.9123			

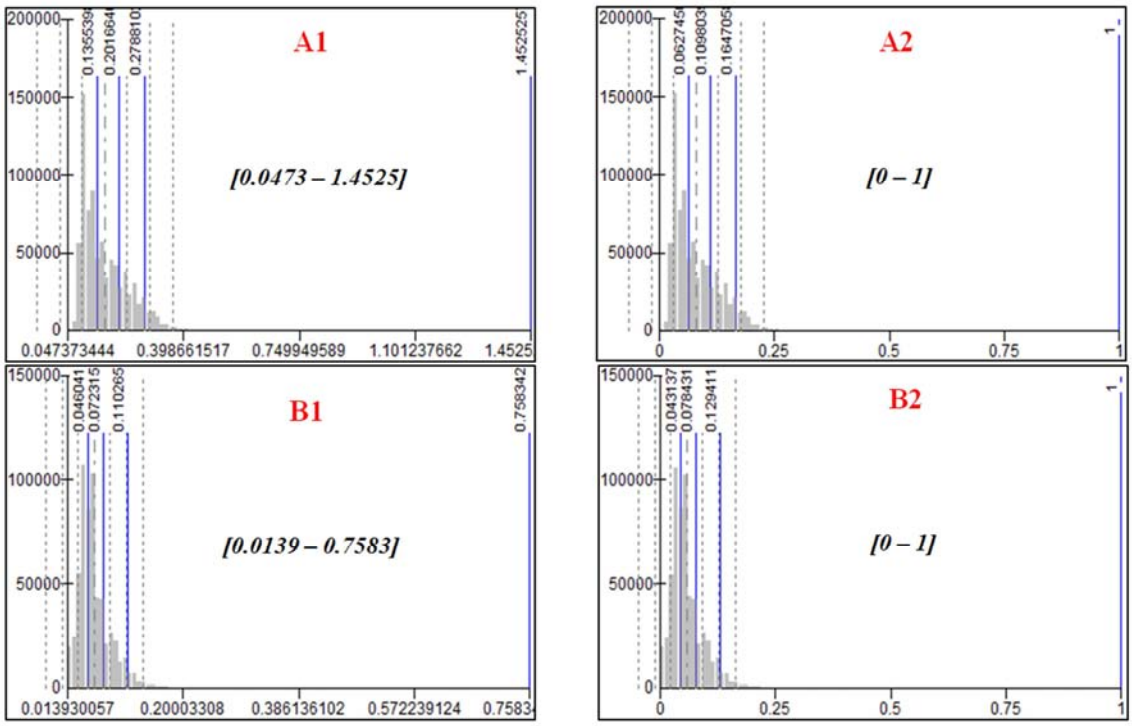

Figure 10. *Snapshots of Jenks natural breaks classes (blue) in Yaoundé (A) and Bangui (B).*

Further, the accuracy assessment was conducted between the unsupervised classification of all the indices compared with RGB classification image used as reference. The random sampling method proposed by [34] was used with 200 locations. The BABI is validated in Yaoundé with an overall accuracy (OA) of 96% and a kappa coefficient (KC) of 0.94, and in Bangui with respectively 98.5% and 0.97 (Table 8). On the two sites, the built-up class is spotted with 100% of OA and 1 of KC, and few water pixels were affected to vegetation class. These scores decrease in the order NDBSUI, MNBI, NDBI and UI in the two cities, due to the generalized built-up detection and the others classes confusion.

Table 8. *Compared accuracy assessment.*

	Yaoundé				**Bangui**			
	PA (%)	***UA (%)***	***OA (%)***	***KC***	***PA (%)***	***UA (%)***	***OA (%)***	***KC***
BABI	95.16	93.8	96	0.94	99.15	95.58	98.5	0.97
NDBSUI	92.59	93.75	93.25	0.9	91.54	87.07	89.18	0.85
MNBI	88.95	87.7	88.46	0.84	92.1	85.4	87	0.82
NDBI	79.18	82.86	87	0.78	89.63	86.95	86	0.81
UI	82.48	81.9	81.3	0.75	88.9	83.01	85.42	0.8

3.2. Biophysical Noise Reduction Ability

According to the second specific goal, the BABI has been able to reduce surroundings brightness and shadowing. The histograms automatically produced for the maps floated [0-1] are monomodal for the BABI, i.e., only one population, assumed to be built-up, is highlighted. The same histograms are bimodal at different degrees for the compared indices, inferring the presence of information other than built-up (Figure 11). In fact, the distribution of the pixels is mathematically assumed to be *normal* (*Gaussian*) and continuous [35]. A full one-peak bell-shaped curve identical to the observation densities (Figure 12), i.e., symmetrical, is considered satisfactory for regrouping similar pixels.

Based on a subset of 50,000 pixels described in ten classes, densities are concentrated between the first five classes, the standard error $SE = 0$, $p < 0.0001$ and $\alpha = 0.05$. The density distribution describes a full bell-shaped curve slightly right-skewed (positive skewness), with $\mu = 0.268$ and $\sigma = 0.065$ in Yaoundé, for $\mu = 0.283$ and $\sigma = 0.04$ in Bangui. The histogram limits the highest peaks in the tight bounds [0.2-0.4], which confirms the lower stretching of the image. This distribution fitting explains the noise reducing, a low confusion between LULC classes and consequently the neat separation of the built-up from surrounding features as pointed out by the accuracy assessment. Comparatively as shown in figure 13, the MNBI and NDBSUI trends are less stretched as for the BABI, their densities are concentrated with bell-shaped curves and their parameters (μ and σ) are low. While the densities of the UI and NDBI are widely stretched, with bell-shaped curves evolve around two to four distribution peaks, and their parameters are higher than BABI ones. These statements support higher trends of classes confusion in other indices, although the MNBI and NDBSUI results are close to the BABI one.

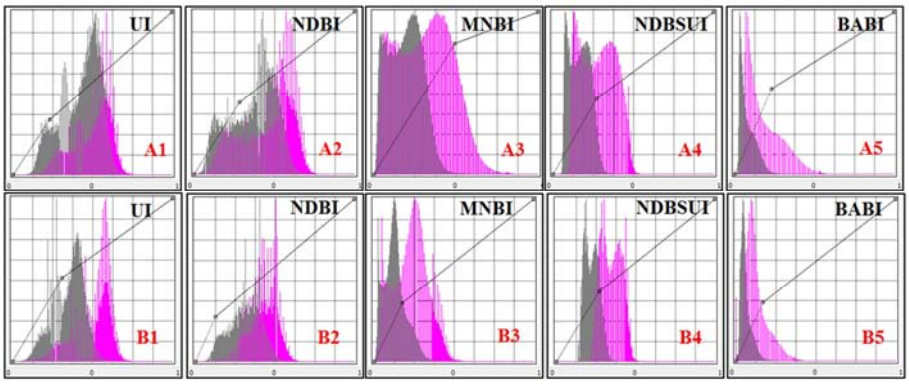

Figure 11. *Automatic density and frequency distribution in Yaoundé (A) and Bangui (B).*

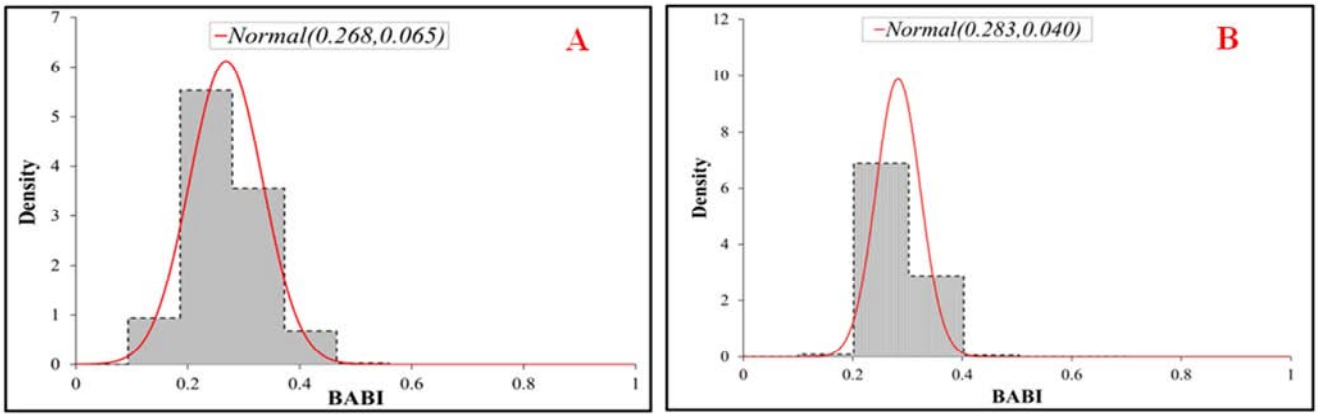

Figure 12. *50,000 sampled pixels' density distribution of BABI in Yaoundé (A) and Bangui (B).*

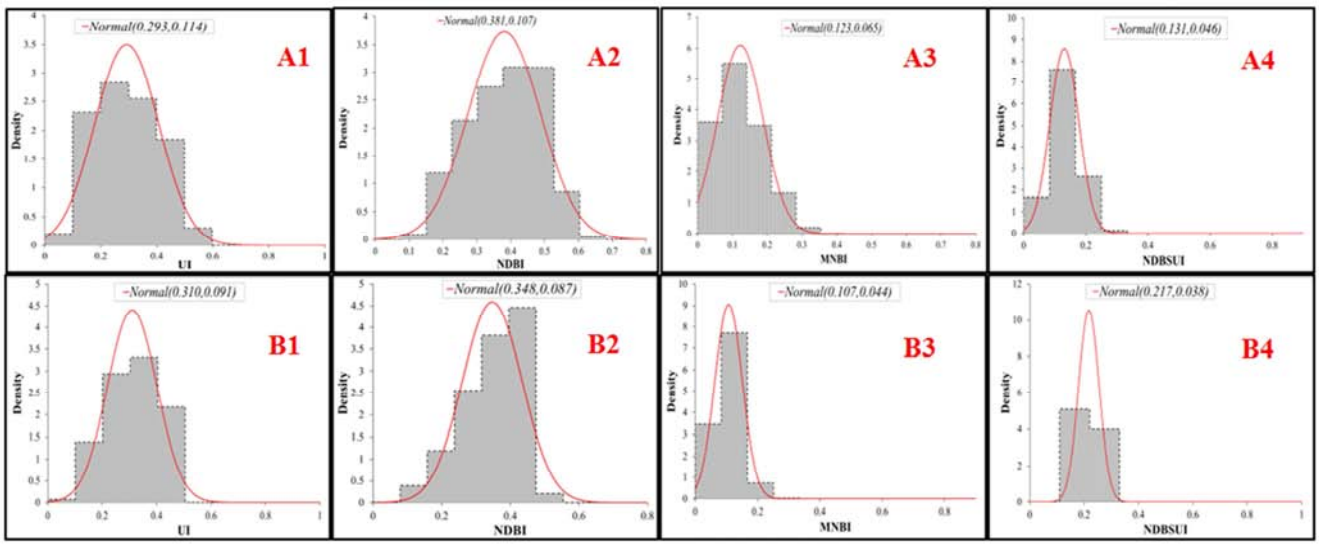

Figure 13. *50,000 sampled pixels' spectral indices density distribution in Yaoundé (A) and Bangui (B).*

4. Discussions

To come up with the BABI, it was tested that urban land surface brightness mixes environmental and built-up information. Using another set of manipulations using the 8-bits recoded results of BABI and comparative indices, one can noticed that the built-up values are higher than those of the other land cover objects, although there are two cases of stretching (Figure 14). In Yaoundé where the forest cover has considerably decreased, exposing rough hilly slopes and rocky soils, all the LULC objects are detected in the high values and close to each other in the stretching interval [125-225]. Whereas in Bangui presenting an important forest coverage, less bare soil visibility, more shadowy rough high-altitude terrain and an important stream of the Ubangui river, LULC

objects are detected in lower values in between the stretching interval [15-185].

On 500 pixels extracted in the highest urbanized area with mixed LULC classes BABI, NDSI/BSI, shadow index and NDISI, the trends confirm the separation between objects. Therefore, built-up can be detected in high or low values in comparison with other LULC spectral indices. As shown in figure 14, trends of BABI are closed to SI but higher than NDSI, while NDISI has the lower values in Yaoundé. For Bangui, trends of the BABI are the lowest, while BSI, SI and NDISI are higher. As the BABI better separates LULC object features, NDISI can be otherwise complementary in detecting dark built-up features (in Yaoundé) and natural impervious surfaces (in Bangui) than effective buildings, as it is closer to soil (NDSI/BSI) and shadow (SI) features.

Finally, BABI is regressed by soil indices, i.e., NDSI/BSI and the Shadow Index, to assess its relation with noise. The r^2 values are the following (Figure 14 & Table 9):

i) In Yaoundé, for BABI/NDSI, $r^2 = -0.42$ and for BABI/SI, $r^2 = 0.24$, for an average $r^2 = 0.33$, lower than compared built-up indices.

ii) In Bangui, for BABI/BSI, $r^2 = 0.55$ and for BABI/SI, $r^2 = -0.59$ for an average $r^2 = 0.57$, that is also lower than other indices.

As the high correlation coefficients were assumed to express the level of noise between and around the built-up area, these lower values are another set of proofs supporting the efficiency of BABI to discriminate built-up from surrounding features.

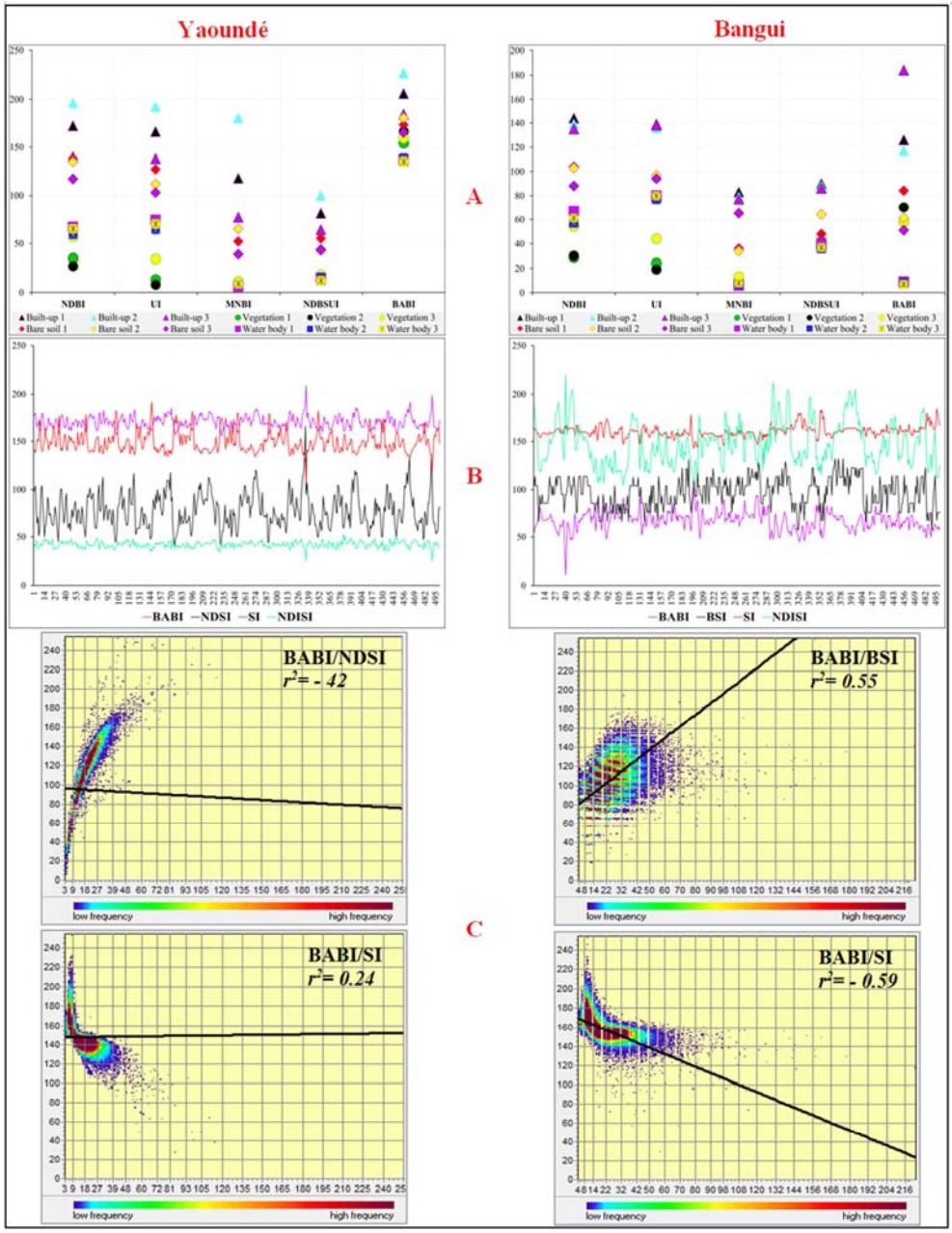

Figure 14. *Post-processing spectral and statistical noise reduction efficiency of BABI.*

Table 9. *Compared r^2 values standing for the post-processing noise prediction.*

	Yaoundé			Bangui		
	Bright noise (NDSI)	***Dark noise (SI)***	***|Average|***	***Bright noise (BSI)***	***Dark noise (SI)***	***|Average|***
NDBI	0.96	- 0.85	0.9	0.77	- 0.84	0.8
UI	0.88	- 0.82	0.85	0.81	- 0.74	0.77
MNBI	0.88	- 0.64	0.76	0.72	- 0.75	0.73
NDBSUI	0.48	- 0.41	0.44	0.71	- 0.6	0.65
BABI	- 0.42	0.24	0.33	0.55	- 0.59	0.57

5. Conclusion

The main goal of this research has been to reduce the land surface brightness and shadow noise that is very challenging for the built-up extraction in unplanned cities with mixed housing materials. The Brightness Adjusted Built-up Index, BABI, gives an improved visual layout with low built-up generalization, confirmed by overall accuracies of 96% and 98.5% respectively in Yaoundé (Cameroon) and Bangui (Central African Republic), way higher than the four comparative spectral indices. Ongoing improvements consist in conducting the full process using a neural network. Further, the computation of BABI was tested in some urban subsets of Sentinel 2 satellite images with satisfactory results, but could not be completed for both whole areas of study because of clouds coverage. Presently, some tests are being conducted for other areas outside the tropics. One advantage of this method can be its potential integration in the population and housing census process of developing countries with low budget allocated. Thus, the BABI may represent an asset for an accurate mapping of human settlements and a better delineation of counting zones using freely accessible satellite images.

Acknowledgements

The private consulting firm StatsN'Maps, through its *'Research Support Funds'* rsf-2-2020 (SN'M-RSF), supported the purchase of articles and books on sale, as well as the article processing charges. The licenses of Erdas Imagine 2020 version 16.6.0.1366, ArcGisPro version 2.5 and XLStats 2020.1.64570 software used for the research were purchased by StatsN'Maps and available upon request. The authors are also grateful to the laboratories of image processing and data analysis of StatsN'Maps, as well as the laboratory of image processing of ILG association for providing and cleaning additional data.

Authors' Contributions

Conceptualization: A. H. N. M. Methodology: A. H. N. M., P. G. G., S. H., R. C., A. F. M. M. and B. N. Data collection and cleaning: A. H. N. M, A. F. M. M. and B. N. Formal analysis and investigation: A. H. N. M. Original draft preparation: A. H. N. M. Review and editing: A. H. N. M., P. G. G., S. H., R. C., A. F. M. M. and B. N. Funding acquisition: A. H. N. M.

Competing interests

The authors declare that they have no competing interests.

References

[1] Esch, T., Heldens, W., Hirner, H., Keil, M., Marconcini, M., Roth, A., Zeidler, J., Dech, S., and Strano, E., Breaking new ground in mapping human settlements from space - The Global Urban Footprint. ISPRS Journal of Photogrammetry and Remote Sensing, 2017, 134, 30-42.

[2] Karlsson, A. Classification of high-resolution satellite images. 2003.

[3] Lu, D. et Weng, Q. A survey of image classification methods and techniques for improving classification performance. International Journal of Remote Sensing, 2007, 28, 823-870.

[4] Masek, J. G., Lindsay, F. E. and Goward, S. N., Dynamics of urban growth in the Washington DC metropolitan area, 1973-1996, from Landsat observation. International Journal of Remote Sensing, 2000, 21, 3473-3486.

[5] Zhang, P., Ke, Y., Zhang, Z., Wang, M., Li, P. and Zhang, S., Urban Land Use and Land Cover Classification Using Novel Deep Learning Models Based on High Spatial Resolution Satellite Imagery. Sensors, 2018, 18, 1-21.

[6] Kawamura, M., Jayamanna, S. and Tsujiko, Y., Relation between social and environmental conditions in Colombo Sri Lanka and urban index estimated by satellite remote sensing data. The International Archives of Photogrammetry and Remote Sensing, 1996, 31, 321-326.

[7] Zha, Y., Gao, J. and Ni, S., Use of normalized difference built-up index in automatically mapping urban areas from TM imagery. *Int. J. Remote Sens*. 24, 583-594 (2003).

[8] Jieli, C., Manchun, L., Liu, Y., Chenglei, S. and Wei, H., Extract residential areas automatically by New Built-up Index. *IEEE*, 2010.

[9] As-syakur, A. R., Adnyana, I. W. S., Arthana, I. W. and Nuarsa, I. W., Enhanced Built-Up and Bareness Index (EBBI) for Mapping Built-Up and Bare Land in an Urban Area. Remote Sensing, 2012, 4, 2957-2970.

[10] Hanqiu, X., Analysis of Impervious Surface and its Impact on Urban Heat Environment using the Normalized Difference Impervious Surface Index (NDISI). Photogrammetry. Engineering and Remote Sensing, 2010, 76, 557-565.

[11] Sun, Z., Wang, C., Guo, W and Shang, R. A Modified Normalized Difference Impervious Surface Index (MNDISI) for Automatic Urban Mapping from Landsat Imagery. Remote Sensing, 2017, 9, (942).

[12] Chen, J., Yang, K., Chen, S., Yang, C., Zhang, S. and He, L., Enhanced normalized difference index for impervious surface area estimation at the plateau basin scale. Journal of Applied Remote Sensing, 2019, 13.

[13] Xu, H. A new index for delineating built-up land features in satellite imagery. International Journal of Remote Sensing, 2008, 29, 4269-4276.

[14] Sinha, P., Verma, N. K. and Ayele, E., Urban built-up area extraction and change detection of Adama municipal area using time-series Landsat images. International Journal of Advanced Remote Sensing and GIS, 2016, 5, 1886-1895.

[15] Ukhnaa, M., Huo, X. and Gaudel, G., Modification of urban built-u area extraction method based on thematic index-derived bands. Earth and Environmental Science, 2019, 227.

[16] Kaimaris, D. and Patias, P. Identification and area measurement of the built-up area with the Built-up Index (BUI). International Journal of Advanced Remote Sensing and GIS, 2016, 6, 1844-1858.

[17] Razul, A., Baltzter, H., Ibrahim, G. R. F., Hameed, H. M., Wheeler, J., Adamu, B., Ibrahim, S. and Najmaddin, P. M. Applying built-up and bare-soil indices from Landsat 8 to cities in dry climates. Land, 2018, 7.

[18] Nichol, J. E., High-resolution surface temperature patterns related to urban morphology in a tropical city: a satellite-based study. Journal of Applied Meteorology, 1996, 35, 135-146.

[19] He, C., Shi, P., Xie, D. and Zhao, Y., Improving the normalized difference built-up index to map urban built-up areas using a semiautomatic segmentation approach. Remote Sensing Letters, 2010, 1, 213-221.

[20] Streutker, D. R. A remote sensing study of the urban heat island of Houston, Texas. International Journal Remote Sensing, 2002, 23.

[21] Mohamed, A. A., Odindi, J. and Mutanga, O., Land surface temperature and emissivity estimation for Urban Heat Island assessment using medium- and low-resolution space-borne sensors: A review. Geocarto International, 2017, 32, 455-470.

[22] Li, E., Du, P., Samat, A., Xia, J. and Che, M., An automatic approach for urban land-cover classification from Landsat-8 OLI data. International Journal Remote Sensing, 2015, 36, 5983-6007.

[23] Slonecker, E. T., Jennings, D. B. and Garofalo, D., Remote sensing of impervious surfaces: a review. Remote Sensing Reviews, 2001, 20, 227-255.

[24] Gbetkom, P. G., Gadal, S., El Aboudi, A., Ngandam Mfondoum, A. H., et al. Mapping of built-up areas in Cameroonians shores of lake Chad and its hinterland through based object classification of Sentinel 2 images. Proceedings of GEOBIA conference, *"From pixels to ecosystems and global sustainability"*, Montpellier, France, 18-22 June, 2018.

[25] Shukla, J. and Mintz, Y. Influence of land-surface evapotranspiration on the earth's climate. Science, 1981, 215, 1498–150.

[26] Brubaker, K. L. and Entekhabi, D. Analysis of feedback mechanisms in land-atmosphere interaction. Water Resources Research, 1996, 32, 1343–1357.

[27] Mustafa, E. K., Liu, G., Abd El-Hamid, H. and Kaloop, M. R., Simulation of land use dynamics and impact on land surface temperature using satellite data. Geojournal, 2019.

[28] Ahmed, B., Kamruzzaman, Md., Zhu, X., Rahman, S. Md and Choi, K., Simulating land cover changes and their impacts on land surface temperature in Dhaka, Bangladesh. Remote Sensing, 2016, 5, 5969–5998.

[29] Bernales, A. M. J., Antolihao, J. A., Samonte, C., Campomanes, F. P., Rojas, R. J., Dela Serna, A. M. and Silapan, J., Modelling the relationship between land surface temperature and landscape patterns of land use land cover classification using multi linear regression models. The International Archives of the Photogrammetry, Remote Sensing and Spatial Information Sciences, 2016, XLI-B8.

[30] Rikimaru, P. S. Roy and S. Miyatake., Tropical forest cover density mapping. Tropical Ecology, 2002, 43, 39–47.

[31] Deng, Y., Wu, C., Li, M. and Chen, R., RNDSI: a ratio normalized difference soil index for remote sensing of urban/suburban environments. International Journal of Applied Earth Observation and Geoinformation, 2015, 39, 40-48.

[32] Ngandam Mfondoum, A. H., Gbetkom, P. G., Cooper, R., Hakdaoui, S. and Wokwenmendam Nguet, P., Assessing the spatial metabolism of a mid-urban/mid-rural city: the relationship built-up, vegetation, bare soil and urban heat in Foumban (west-Cameroon, Central Africa) – periods 1987-2003-2019. *Proceedings of the 3rd International Land Use Symposium, ILUS, "Land use changes: trends and projections"*, Paris, France, 4-6 December, 10.13140/RG.2.2.13421.33766, 2019.

[33] Ngandam Mfondoum, A. H., Gbetkom, P. G., Cooper, R., Hakdaoui, S. and Mansour Badamassi, M. B., Extraction of Built-up features in complex biophysical environments by using a Landsat bands ratio. The International Archives of the Photogrammetry, Remote Sensing and Spatial Information Sciences, 2020, XLIV-M-2-2020, 79-85.

[34] Congalton, R. G. and Green, K. Assessing the Accuracy of Remotely Sensed Data-Principles and Practices. 2nd ed. CRC Press: Boca Raton, FL, USA, p. 183, 2009.

[35] Schowengerdt, R. A. Remote Sensing, Models, and Methods for Image Processing. Academic Press, p. 522, 1997.

[36] Zhao, H., Chen, X. and Tian, L., A new method to retrieve topographic shadow based on multi-spectral operation. *IEEE*, 2006, 2750-2753.

[37] Chavez, P. S. Image-based atmospheric corrections–revisited and improved. Photogrammetry Engineering and Remote Sensing. 1996, 9, 1025–1036.

[38] Barsi, J. A., Schott, J. R., Hook, S. J. Raqueno, N. G., Markham, B. L. and Radocinski, R. G., Landsat-8 thermal infrared sensor (TIRS) vicarious radiometric calibration. Remote Sensing, 2014, 6, 11607–11626.

[39] United States Geological Survey. Landsat 8 (L8) data users handbook version 5.0. P. 106, 2019.

[40] Barsi, J. A., Lee, K., Kvaran, G., Markham, B. L. and Pedelty, J. A., The Spectral Response of the Landsat-8 Operational Land Imager. Remote Sensing, 2014, 6, 10232-10251.

[41] Lu, D. and Weng, Q. Use of impervious surface in urban land-use classification. Remote Sensing of the Environment, 2006, 102, 146-160.

[42] Wu, C. and Murray, T. Estimating impervious surface distribution by spectral mixture analysis. Remote Sensing of the Environment, 2003, 84, 493-505.

[43] Lu, D., Moran, E. and Hetrick, S. Detection of impervious surface change with multitemporal Landsat images in an urban-rural frontier. ISPRS Journal of Photogrammetry and Remote Sensing, 66, 298-306.

[44] Moayedi, H.; Rezaei, A. An artificial neural network approach for under-reamed piles subjected to uplift forces in dry sand. Neural Computing and Applications, 2019, 31, 327–336.

[45] Moayedi, H.; Hayati, S. Applicability of a CPT-Based Neural Network Solution in Predicting Load-Settlement Responses of Bored Pile. International Journal Geomechanics, 2018, 18.

[46] Rosenblatt, F., Principles of Neurodynamics: Perceptrons and the Theory of Brain Mechanisms. Spartan Books, Washington, DC, 1961.